Earth-Science Reviews 138 (2014) 454–468

Contents lists available at ScienceDirect

Earth-Science Reviews

journal homepage: www.elsevier.com/locate/earscirev

Stress, strain and mass changes at Mt. Etna during the period between the 1991–93 and 2001 flank eruptions

Daniele Carbone [a,*], M. Aloisi [a], S. Vinciguerra [b,c], G. Puglisi [a]

[a] Istituto Nazionale di Geofisica e Vulcanologia, Sezione di Catania — Osservatorio Etneo, Catania 95125, Italy
[b] Department of Geology, University of Leicester, Leicester LE1 7RH, United Kingdom
[c] British Geological Survey, Keyworth, Nottingham NG12 5CG, United Kingdom

ARTICLE INFO

Article history:
Received 12 March 2014
Accepted 16 July 2014
Available online 25 July 2014

Keywords:
Etna volcano
Gravity changes
Ground deformation
Fracture zone
Young's modulus
Finite element method

ABSTRACT

During the ~8-year period between the 1991–93 and 2001 flank eruptions, the eruptive activity of Mt. Etna was confined to the summit craters. Deformation and tomography studies indicate that this activity was fed by a magma accumulation zone centered NE of the summit, at a depth of 5 to 9 km below sea level. The most significant gravity changes measured during the same period were induced by mass redistributions at shallower depth below the south-eastern flank of the volcano, where minor ground deformation was observed (i.e., vertical displacements within 2 cm). The mismatch between the position of pressure and mass sources is difficult to explain under the assumption that both are directly related to magma dynamics. Past studies have suggested that the gravity changes observed during 1994–2001 may primarily reflect changes in the rate of microfracturing along the NNW–SSE fracture/weakness zone (FWZ) that crosses the SE slope of Etna.

We use the finite element method to shed new light on the complex relations between stress, strain and mass changes that occurred at Etna during the studied period. In particular, following previous results on the degradation of the mechanical properties of rocks, we perform a set of simulations assuming that the part of the medium containing the FWZ is characterized by a lower Young's modulus than would be expected from interpolation of tomographic data. We find that the presence of the FWZ creates a distortion of the displacement field induced by the deeper pressure source, locally resulting in a weak extensional regime. This finding supports the hypothesis of a cause–effect relationship between pressurization beneath the NW flank and tensile extension beneath the SE slope of the volcano. We propose that this extensional regime enhanced the propagation of pressurized gas, that, in turn, amplified the tensile strain across the FWZ.

We also find that decreasing the value of Young's modulus in the FWZ allows for a larger amount of extension at depth, with no change in the magnitude of surface displacements. This result provides an indication of how the changes in the rate of microfracturing at depth, which are needed to induce the observed gravity changes, might have occurred without large ground deformation.

Contents

* Corresponding author. Tel.: +39 095 7165800; fax: +39 095 435801.
E-mail address: carbone@ct.ingv.it (D. Carbone).

http://dx.doi.org/10.1016/j.earscirev.2014.07.004

1. Introduction

Volcanic eruptions are commonly thought to be initiated by overpressure in the magma chamber, leading to the intrusion of magma batches that force their way through the volcanic edifice and to the surface (Blake, 1981; Tait et al., 1989). Geophysical evidences demonstrated that this mechanism of ascent is the cause of eruptions from different volcanoes (Linde et al., 1993; Poland et al., 2009). In some cases, however, the heuristic model linking volcanic eruptions to forceful magma intrusions through the volcanic edifice is not supported by available observations (Branca et al., 2003; Scandone et al., 2007). For example, at some volcanoes (e.g., Mt. Pinatubo, Mt. St. Helens), shallow seismicity with randomly distributed hypocenters, rather than upward migration of hypocenters, suggestive of forceful magma injection, has been observed prior to eruptive events (Malone et al., 1983; Harlow et al., 1996).

The mechanisms allowing magma transport may be complicated by the interplay between magmatic activity and the stress field acting on the embedding medium (Pinel and Jaupart, 2000). Indeed, while the local stress field may be modified by magma pressure, changes in the characteristics of the host medium can have a significant impact on magma transport from deep storage zones to the surface (Famin and Michon, 2010). The existence of such complex relations between magmatic activity and the local stress field has been investigated through experimental studies based on geophysical data. In particular, measurement of the travel time of seismic waves has been used to detect perturbations in the elastic proprieties of a volcanic edifice induced by modifications in the local stress field (e.g. Ratdomopurbo and Poupinet, 1995). For example, Brenguier et al. (2008) used continuous ambient seismic noise records to detect temporal decreases of seismic velocities within Piton de la Fournaise volcano (La Réunion). They interpreted these velocity decreases as the dilatation responses of the edifice to changes in the stress field, in turn due to phases of magma pressurization. Hautmann et al. (2010) observed gravity changes at Soufrière Hills Volcano (Montserrat, West Indies), centered about 7 km from the eruptive vent. The authors suggested that these anomalies were due to changes in the fracturing rate along a hitherto unrecognized fault zone and proposed that changes in the stress field around the shallow plumbing system of the volcano induced the inferred fracturing.

Over the past decade, the rapid growth of computational power has allowed for increasingly detailed and complex modeling studies. Numerical approaches have been used to investigate possible relations between magmatic activity and the stress field (e.g. Walter et al., 2005; Manconi et al., 2007; Hautmann et al., 2009; Gerbault et al., 2012; Privitera et al., 2012).

Mt. Etna (Italy) is a Quaternary polygenetic volcano located on the east coast of Sicily (Fig. 1). It lies in a complex geodynamic setting where (i) an almost east–west extensional regime, recorded by the NNW–SSE-trending transtensional Timpe fault system (Fig. 1), and (ii) a north–south compressive regime, related to the southward migration of the Apennine–Maghrebian chain (Catalano et al., 2004), are simultaneously active (Bousquet and Lanzafame, 2004). The volcano's sector prone to seaward sliding (eastern to southern flanks; Bonforte et al., 2011) is delimited by the E–W-trending Pernicana fault system to the

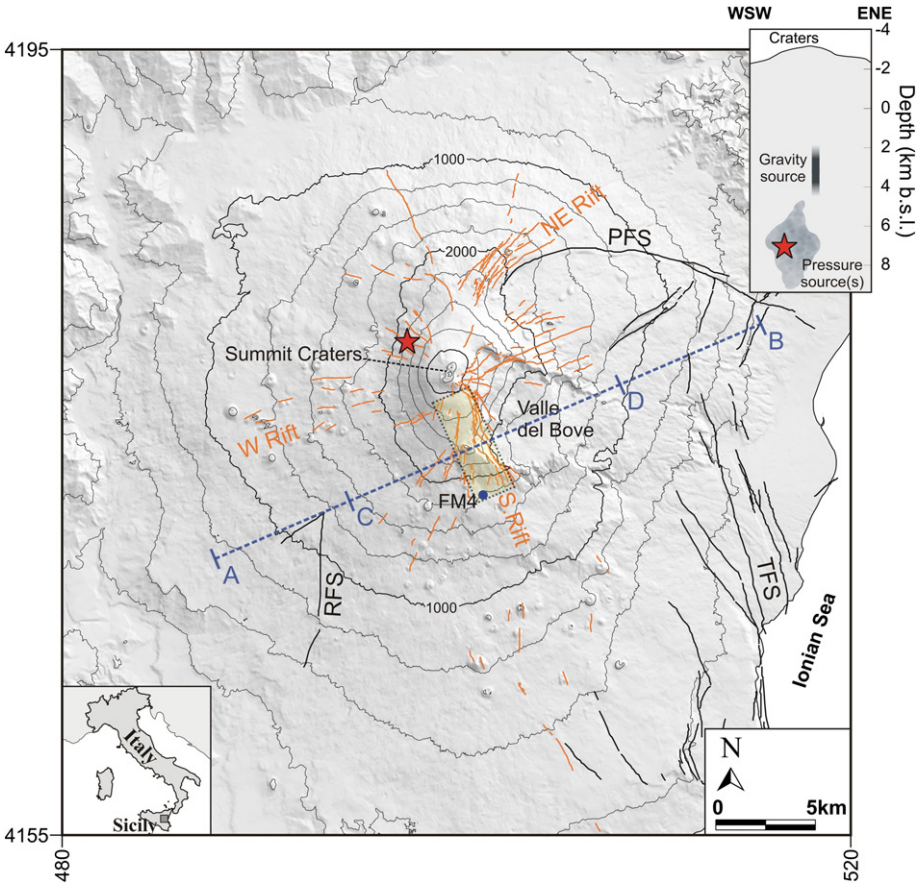

Fig. 1. Map of Mount Etna. Yellow box: surface projection of the volume assumed to contain the FWZ (see text for details). Red star: projected position of the pressure source active during the period under study (see text for details). Black lines: main faults (PFS: Pernicana fault system, TFS: Timpe fault system, RFS: Ragalna Fault System). Orange lines: main eruptive fissures. Dashed blue line: trace of the cross-sections presented in Figs. 4, 7 and 8. The inset at the top right shows a cross section along a profile parallel to the northernmost portion of the dashed red line and crossing the summit crater zone. The shaded gray area in the inset indicates the position of the pressure source active during the 1994–2001 period (from Bonforte et al., 2008; the red star is the averaged position assumed in the present study).

NE and by the N–S-trending Ragalna fault system to the SE (Fig. 1), characterized by left-lateral and right-lateral motion, respectively.

Recent volcanic activity has been mainly focused on the summit craters and along fissures on the flanks that, in the upper part of the volcano, are mostly clustered in three main rift zones, namely, the NE, S, and W rifts (Fig. 1). The NE and S rifts are kinematically connected to the Pernicana and Ragalna fault systems, respectively (Falsaperla et al., 2010; Solaro et al., 2010). During the last decades, Mt. Etna has exhibited various eruptive styles, ranging from strongly explosive to quietly effusive (Allard et al., 2006). Different patterns of precursory signals have preceded the paroxysmal events, suggesting that different mechanisms have allowed magma to rise to the surface (from "passive" magma ascent along pre-existing open spaces to forceful intrusions into the rift zones; Patanè et al., 2005; Bonforte et al., 2008). Past studies provided evidence supporting the view that the interplay between magma dynamics and the thermomechanical response of the host medium exerts considerable control on the eruptive activity of Mt. Etna, implying that a deep understanding of the underlying processes requires consideration of a range of observables (e.g. Aloisi et al., 2011).

Carbone et al. (2009) analyzed gravity and seismic data acquired at Etna and detected, during the time interval between major flank eruptions in 1991–93 and 2001, a marked coupling between mass changes and release of seismic energy, over both time and space (Fig. 2). In particular, the phases of gravity decrease (late-1996 to mid-1999 and late-2000 to mid-2001) occurred during increases in the release of seismic energy (panels c, d and f of Fig. 2) and were interpreted as due to changes in the rate of micro-fracturing along the NNW–SSE fracture/weakness zone (hereafter referred to as FWZ) that cuts the SE flank of the volcano (Fig. 1). The FWZ follows the trend of the upper S rift (Fig. 1), whose surface expressions in the last decades are given by the dry

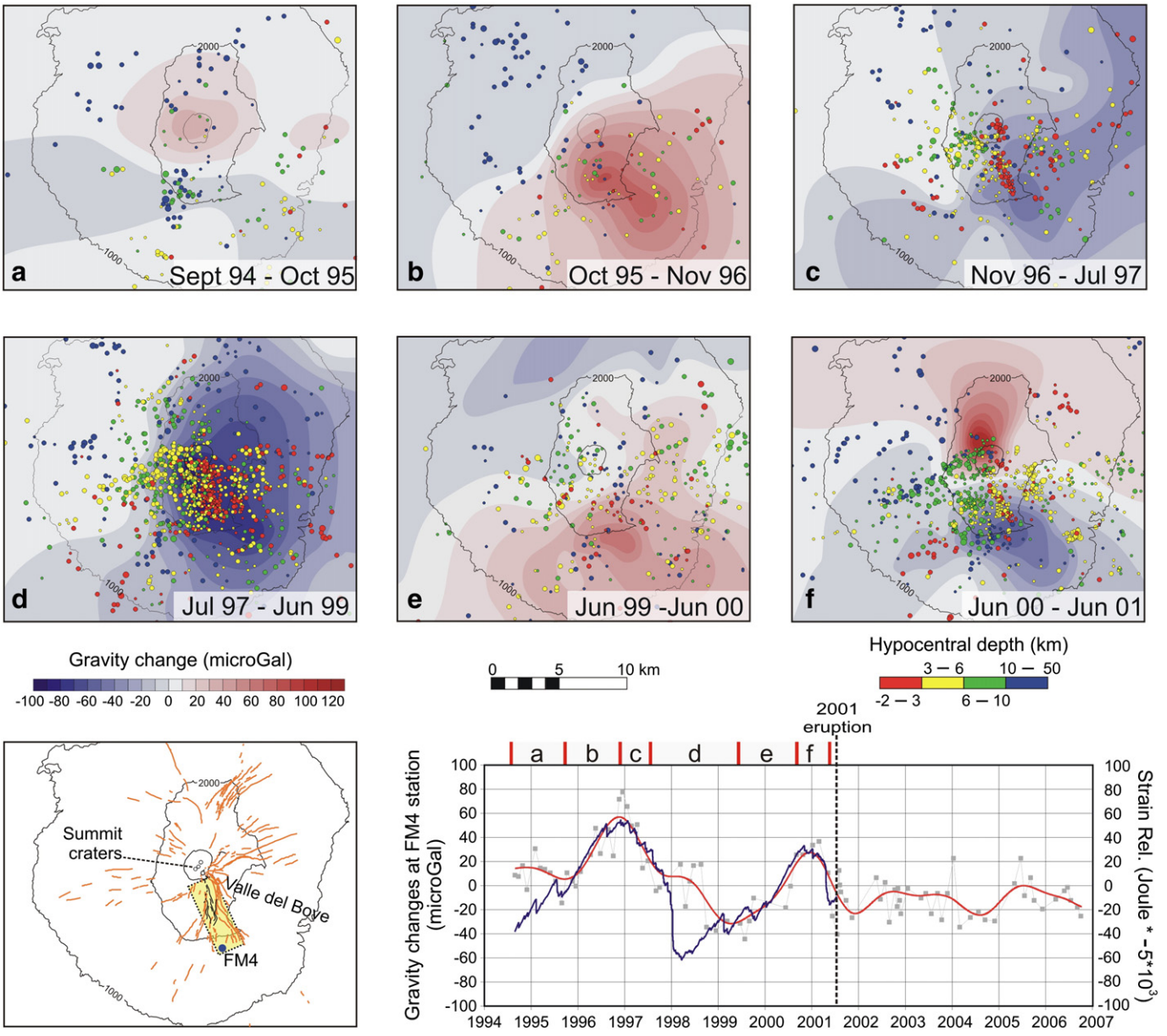

Fig. 2. Panels a–h: sketch maps showing gravity changes and earthquake epicenters for different time intervals. Hypocentral depth ranges are indicated by color. Gravity changes are contoured at 10 μGal intervals. Bottom left panel: map showing the position of the FM4 gravity station, the surface projection of the FWZ (yellow box) and the main eruptive fissures (orange lines; black lines indicate fissures that opened during the 2001 eruption). Bottom right graph: temporal changes in gravity observed at the FM4 station during the 1994–2006 period (gray squares). The red curve is the same sequence corrected for the water-table effect (see Carbone et al., 2009) and low-pass filtered with a cut-off period of about 2.5 years. The solid blue curve is the seismic strain release after removal of a linear trend and multiplication by a negative coefficient ($-5 * 10^{-4}$). Redrawn from Carbone et al., 2009.

fractures which opened during the 1989 eruption and/or the eruptive fissures of the 1991–93 and 2001 eruptions (Calvari et al., 1994; Allard et al., 2006; Corsaro et al., 2007; Falsaperla et al., 2010). The FWZ is also likely part of the structural trend that can be traced southwards along the Timpe fault system and, at a larger scale, along the "Malta Escarpment" lithospheric fault. The latter borders the eastern margin of Sicily and crosses the volcano, controlling its mainly tensional tectonic regime (Bousquet and Lanzafame, 2004). An increase in the rate of fracturing along the FWZ implies an increase in the release of seismic energy and induces "*medium rarefaction*" (Carbone et al., 2009), which is associated with a local density (gravity) decrease. The mechanism proposed by Carbone et al. (2009) could thus explain the observed coupling between gravity and seismic data. The 2001 phase of gravity decrease/strain-release increase (panel f and bottom graph in Fig. 2) culminated in the breakout of the 2001 flank eruption (Carbone et al., 2003a) and it was proposed that pressurized magma in a deeper reservoir used the zone of increasing microfracturing as a path to reach the surface (Puglisi et al., 2008; Carbone et al., 2009). This process would therefore represent the other side of the above evocated feedback loop: while magmatic activity resulted in mechanically- and thermally-induced medium fracturing, the developing fracture network eventually allowed magma rise to the surface.

The framework proposed by Carbone et al. (2009) is the starting point of the present study, which aims to provide a better understanding of the processes that acted during the 1994–2001 period and that led to the 2001 flank eruption. In particular, we use a finite-element modeling (FEM) approach to shed light on (i) the mechanism controlling the inferred changes in the rate of microfracturing within the NNW–SSE FWZ and (ii) the relation between volume changes at depth and deformation of the ground surface.

2. The period between the 1991–93 and 2001 major flank eruptions of Etna

The 1991–1993 flank eruption took place from a vent in the SW wall of the Valle del Bove (Calvari et al., 1994) and was the most important at Etna in the last 300 years, both in terms of duration (472 days) and volume of lava emitted (about $235 * 10^6$ m^3). After this eruption and until July 1995, Etna's activity consisted of non-eruptive degassing from the summit craters (Behncke et al., 2006). From late July 1995, an almost continuous activity, confined to the summit vents, took place and increased in intensity over time until June 2001. The summit craters exhibited a wide range of eruptive styles, including effusive activity, strombolian explosions and sequences of powerful lava fountains (see Allard et al., 2006 and references therein). With the breakout of the July–August 2001 eruption a new phase of Etna's activity started, consisting of four successive flank eruptions, accompanied by a dramatic reduction in the activity from the summit craters (Neri et al., 2005).

Geophysical data collected during the time interval between the 1991–93 and 2001 main flank eruptions of Etna were the focus of many studies aimed at describing the coupled processes that controlled the volcanic activity (Bonaccorso and Patanè, 2001; Alparone et al., 2003; Allard et al., 2006; Bonaccorso et al., 2011).

Ground deformation studies based on GPS and InSAR data (Puglisi et al., 2001; Bonforte and Puglisi, 2003; Lundgren et al., 2003; Houlié et al., 2006; Bonforte et al., 2008; Palano et al., 2008; Trasatti et al., 2008; Solaro et al., 2010; Bonforte et al., 2011) indicate that, after the 1991–93 eruption, Mt Etna entered a continuous and fairly constant inflation phase that lasted until the start of the 2001 eruption. Inflation was driven by a pressure source (or family of sources) located below the western flank of the volcano (Fig. 1) at a depth between 5 and 9 km b.s.l. (top-left inset in Fig. 1; see Bonforte et al., 2008 and references therein). During the same period, the overall pattern of ground deformation was influenced by the seaward sliding of the eastern flank of the volcano, mainly driven by gravity instability (Bonforte and Puglisi, 2003, 2006; Palano et al., 2008), but also boosted by factors like heterogeneities within the edifice, topography and the presence of magmatic sources (e.g., Aloisi et al., 2011; Chiocci et al., 2011; Cianetti et al., 2012).

The analysis of gravity data from repeated campaigns revealed that, during the 1994–2001 period, the most important mass redistributions occurred within an elongated source-volume beneath the SE flank of the volcano. The only gravity anomalies outside that sector were observed in the summit zone of the volcano and reflect local short-term changes associated with the magma dynamics in the shallowest part of Etna's plumbing system. An example is given by the short-wavelength increase observed during the second half of 2000 in the summit zone of the volcano (positive anomaly in panel f of Fig. 2) and interpreted as due to magma accumulation at about 1.5 km below the summit craters (Carbone et al., 2003a, 2009). Early research based on gravity data from Etna (Budetta et al., 1999; Carbone et al., 2003b) proposed that the 1994–99 sequence of gravity increase and decrease (panels a–d of Fig. 2) reflected the flow of a large volume of magma (3 to $10 * 10^8$ m^3) that emplaced at shallow depth below the SE flank of the volcano, before degassing and sinking to deeper parts of the plumbing system — a view that was echoed in more recent studies (Greco et al., 2010; Bonaccorso et al., 2011). With the observation of (1) the further gravity increase/decrease (1999–2001; panels e and f of Fig. 2), that culminated with the 2001 flank eruption (Carbone et al., 2003a), and (2) the coupling between gravity and strain release changes (Fig. 2; Carbone et al., 2009), an alternative interpretation was put forward that all the gravity changes observed during 1994–2001 in the southeastern sector of Etna may primarily reflect changes in the rate of microfracturing of the medium, rather than being a direct effect of magma movements. The latter interpretation is supported by the following arguments:

(i) it allows to explain why the main 1994–2001 mass changes occurred in a sector peripheral to the trajectories of magma migration from the deep storage to the surface (De Gori et al., 2005);
(ii) it provides a conceptual framework for understanding the coupling between gravity and seismic data before the onset of the 2001 eruption (Carbone et al., 2009);
(iii) it agrees with petrological and volcanological evidence that indicates a fast rise, from a deep storage to the surface, of most magma discharged during the 2001 eruption (Pompilio et al., 2001; Corsaro et al., 2007).

With reference to the last point above, the fast ascent of the magma erupted from the vents at lower elevations may have been facilitated by the zone of increased microfracturing, which served as a path to reach the surface (Carbone et al., 2003a, 2009).

If interpreted as due to magma movements, the 1994–2001 gravity changes would imply the flux of a large amount of magma through a peripheral sector of the volcano — an implication that is not supported by independent evidence. Bonaccorso et al. (2011) claimed that the ratio between (a) amount of magma discharged during the 1995–2003 period and (b) deep magma flux implied by the 1994–99 gravity changes matches the ratio of degassed to erupted magma deduced from geochemical data (Allard, 1997; Allard et al., 2006). This conclusion, however, is not adequately supported because it is based on a calculation that does not take into account the gravity changes during the 1999–2001 period (panels e and f of Fig. 2), pointing to a further mass change of about $2.5 * 10^{11}$ kg (Carbone et al., 2003a). Furthermore, Bonaccorso et al. (2011) concluded that the magma emitted until 2003, including the 2001 and 2002–03 flank eruptions, came from the relatively shallow accumulation zone (they report a depth between 1.8 and 2.5 km b.s.l.) that formed between 1994 and 1997. This conclusion implies years-long storage at shallow depths and thus contradicts petrological and volcanological evidence (Pompilio et al., 2001; Corsaro et al., 2007) suggesting that most of the magma emitted during the 2001 eruption was a primitive, gas-rich magma that ascended rapidly to the surface from a deeper reservoir.

While it is unlikely that a large amount of magma fluxed through the SE sector of the volcano during the 1994–2001 period, it cannot be

discounted that limited episodes of magma injection from the central conduit to the sector enclosing the FWZ took place. In that regard, a discrepancy between gravity and strain release curves can be observed for about one year after January 1998 (bottom graph in Fig. 2). This discrepancy may have been driven by the gravity effect of the shallow magma intrusion that was inferred to have caused the January 1998 seismic swarm (Bonaccorso and Patanè, 2001).

With respect to the results of ground deformation studies, the conclusions reached by Carbone et al. (2003a, 2009) about the sharp mismatch between the position of pressure and mass sources active at Etna during the 1994–2001 period stand in contrast to most previous studies from other volcanoes where a common gravity/deformation source could explain the observations (Battaglia et al., 2003; Bonvalot et al., 2008). By analyzing the distribution of seismicity during the phases of high strain release, Carbone et al. (2009) hypothesized that the mechanical behavior of Etna was not homogeneous and was possibly related to an internal cause–effect relationship. Specifically, they proposed that the extensional dynamics of the upper southeastern flank between 1994 and 2001, which was inferred to be the main source of gravity changes, may represent the response of the FWZ to the deep pressure source below the west flank (the main ground deformation source). Carbone et al. (2009) did not provide quantitative information about the mechanisms behind the proposed cause–effect relationship.

The first aim of the present study is to develop a quantitative understanding of the dynamic interplay between stress changes below the western flank and mass redistributions below the southeastern slope of Etna.

The amount of extension needed across the NNW–SSE FWZ to induce the observed gravity changes via changes in the rate of microfracturing can be calculated through the analytical formulation of Okubo and Watanabe (1989). Their approach is well suited for the task, as it involves uniformly distributed infinitesimal cracks buried in an elastic half-space. Using suitable ranges for the input parameters the analytical model of Okubo and Watanabe (1989) predicts that extension across the FWZ of between 1 and 2 m is needed to explain the 1994–2001 phases of gravity decrease. The same formulation indicates that vertical displacement with amplitude of several cm should also develop, but available geodetic data (e.g. Palano et al., 2008 and references therein) do not support this prediction. Indeed, between 1994 and 2001, vertical displacements in the area where the strongest gravity changes occurred were within 2 cm and probably mostly due to a pressure source beneath the NW flank of the volcano (Palano et al., 2008; Bonforte et al., 2011). As noted by Carbone et al. (2007), the above discrepancy could depend on the elastic half-space assumption of the Okubo and Watanabe (1989) model. Indeed, the mechanical behavior at depth can be significantly changed by the spatial variability of the medium properties.

The second aim of the present study is to understand whether, once the most significant heterogeneities of the medium are accounted for, the volume changes at depth that are needed to explain the observed gravity changes are consistent with the minor deformation measured at the surface.

3. Numerical modeling

3.1. FEM model

In the framework of the present study, stress and strain quantities are calculated using the finite element modeling (FEM) approach. By dividing the computational domain into small elements, FEM simulations overcome the half-space limitation of analytical solutions — specifically, it is possible to calculate the stress/strain relationship throughout the entire model volume assuming a heterogeneous medium with the real topography (Charco et al., 2009). The 3-D FEM model used in the present study has been developed using the software package COMSOL Multiphysics v4.3a (http://www.comsol.com). The computational domain (Fig. 3) is centered on the summit zone of Etna (504.2 km East and 4179.6 km North; x, y in UTM-WGS84 coordinates) and has a size of $98 \times 98 \times 50$ km^3. This size is large enough to avoid bias from boundaries, along which displacement and stress fields are fixed to zero.

The mesh of the computational domain (Fig. 3) is composed of about 420,000 tetrahedral elements, whose average size ranges between 5 km (in peripheral zones) to 100 m (in the area of interest). The smallest elements are located inside a cubic sub-domain (side = ~12 km), which includes the FWZ and the pressure source (Fig. 3).

At the bottom of the domain the displacement is fixed to zero, while at the outermost lateral boundaries only tangential displacements are allowed, in order to absorb residual displacements (Aloisi et al., 2011). Conversely, the top of the domain, representing the ground surface, is left free to move so that the modeled deformation pattern at the ground surface is free from any a priori assumption. Information on volcano topography is drawn from a digital elevation model (DEM) interpolated from Shuttle Radar Topography Mission data (http://www2.jpl.nasa.gov/srtm/), and has a resolution of 1×1 km. Bathymetry data are taken from Smith and Sandwell (1997).

To test whether near field displacements are suitably reproduced by the numerical scheme, we perform a comparison between exact analytical solutions (McTigue, 1987) and corresponding results of the FEM model for a finite spherical pressure source, assuming a homogeneous computational domain with flat free surface (Aloisi et al., 2011). The analytical and numerical solutions coincide, supporting the accuracy of the FEM results.

3.2. Medium characteristics

The volcanic edifice of Mt. Etna consists of a ~1.5 km-thick basaltic cover that rests upon a large sedimentary basement. The latter comprises a mixture of marly clays, marly limestones and quartz-arenitic rocks (Catalano et al., 2004) from the Maghrebian–Appennine chain that, in turn, overly a thick succession of limestone and dolomite, referred to as the Hyblean Plateau (Lentini, 1982; Grasso and Lentini, 1982; Pedley and Grasso, 1992). The carbonates of the Hyblean Plateau lie at depths greater than about 4 km beneath the volcanic edifice (Tibaldi and Groppelli, 2002; Behncke and Neri, 2003; Lundgren et al., 2004; Andronico et al., 2005) and have an average thickness of about 10 km (see Yellin-Dror et al., 1997 and references therein).

The most common rock in the basaltic pile is a porphyritic intermediate alkali basalt (Tanguy et al., 1997) that typically features an extensive pre-existing network of interconnected microcracks. The cracks have been interpreted as resulting from rapid cooling that is typical of lava flows (Vinciguerra et al., 2005). The stress-induced degradation of the mechanical properties of this lithology was investigated in the laboratory (Heap et al., 2009), where a decrease in the Young's modulus (E) by about 30% (down to 20 GPa) was observed. This behavior was primarily attributed to an increase in the level of crack damage within the samples.

The evolution of the mechanical properties of the rocks forming the sub-volcanic sedimentary substratum of Etna depends on their chemical composition and physical characteristics. Stress-induced damage is augmented by mineralogical, chemical, and textural changes induced by the proximity of high-temperature magmatic sources (Mollo et al., 2012) and can lead to a decrease of E down to ≈5 GPa (Heap et al., 2013).

Results of gravity studies (Budetta et al., 1999; Carbone et al., 2003a; 2003b, 2009) suggest that the FWZ is located at a depth of 2–4 km b.s.l, implying that it is embedded in the sedimentary substratum of Etna. Large magma bodies are known to be present at the same depth, as shown in the results from seismic (Chiarabba et al., 2000; Aloisi et al., 2002; Patanè et al., 2006) and gravity (Schiavone and Loddo, 2007) data.

The NNW–SSE-oriented FWZ is located at the western margin of the solidified magmatic intrusion that underlies the southern part of the Valle del Bove (Aloisi et al., 2002; Schiavone and Loddo, 2007).

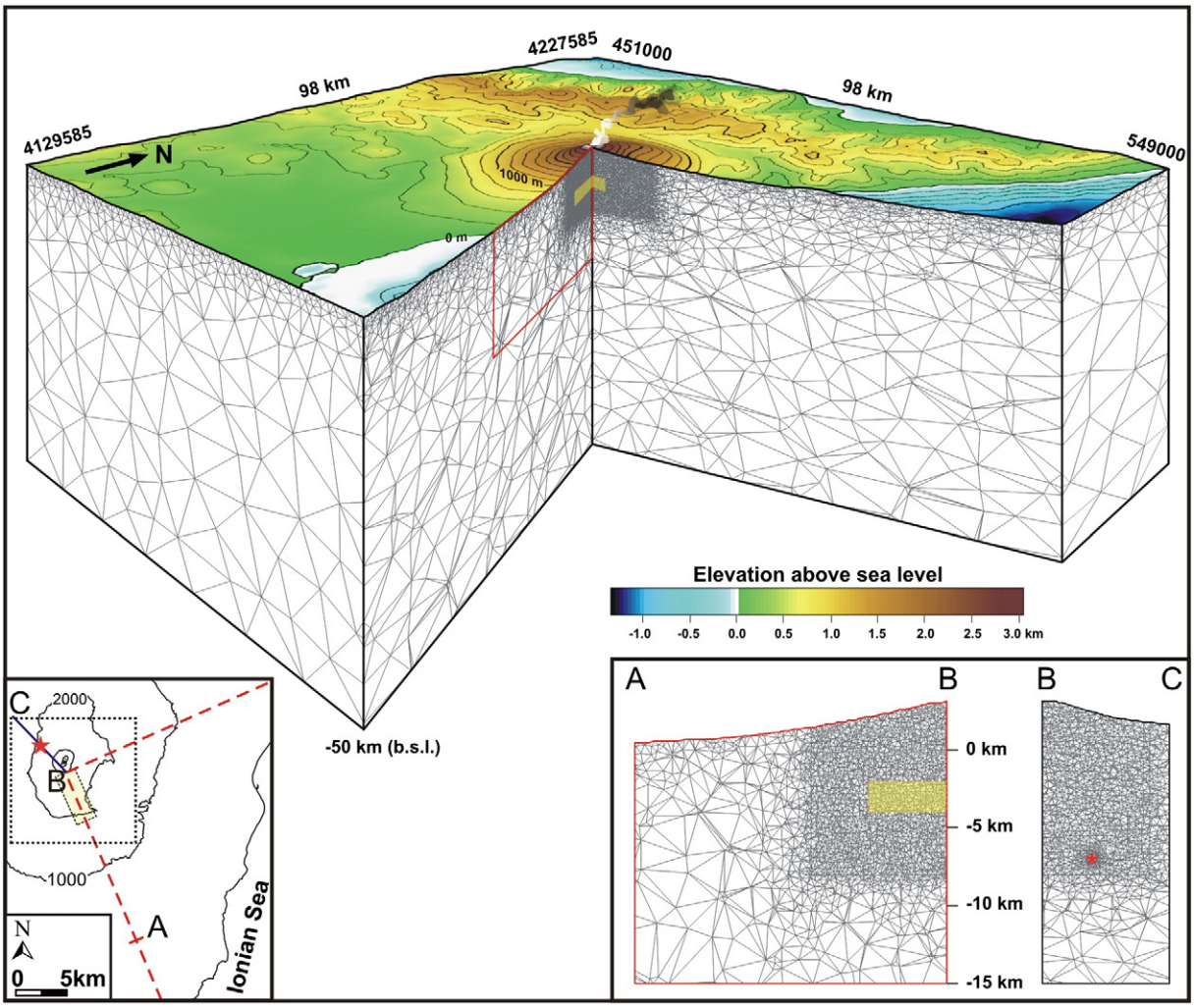

Fig. 3. 3D view of the meshed domain utilized in the present study (cross section along the dashed red trace in the inset at the bottom left). The mesh elements become smaller in size from the margins to the ground surface and the central sub-domain (dotted black line in the inset at the bottom left), including the FWZ (whose projection is marked in yellow) and the pressure source (red star). The inset at the bottom right shows details of the meshed domain along the A–B (area enclosed by the red line in the main panel) and B–C traces shown in the inset at the bottom left.

However, the available tomographic models lack sufficient spatial resolution to determine whether the FWZ cuts through only sedimentary rocks, or through sedimentary rocks with magmatic intrusions.

Based on the above observations, the numeric calculations described in the next sections are performed with allowance for the following points.

(i) We use available data from seismic tomography studies (Aloisi et al., 2002; Patanè et al., 2006) to derive (by linear interpolation among nodes) the elastic parameters of the medium. Outside the volcanic area, where the reliability of the tomographic models is below an acceptable limit (i.e. spread function ≤4; Michelini and McEvilly, 1991), we use the 1-D model of Hirn et al. (1991). The Young's modulus is calculated from seismic-wave velocities using Hooke's relationship (see Aloisi et al., 2002 for a detailed discussion of this topic).

(ii) The position and size of the FWZ are derived from the results of gravity studies (Budetta et al., 1999; Carbone et al., 2003a, 2003b). Following Carbone et al. (2009), we modeled the FWZ as a 2 × 2 × 5 km parallelepiped centered at a depth of 3 km b.s.l.; its position and orientation are shown in Figs. 1 and 3.

(iii) In most calculations we assume a lower value of the Young's modulus in correspondence of the NNW–SSE FWZ than in the surrounding medium (where E values are deduced via interpolation of tomography data). In particular, due to the above uncertainties about the lithologies cut by the FWZ and their physical state, values of E ranging between 5 and 25 GPa are assumed in the simulations described in the following sections.

4. Results of the numerical analysis

4.1. Distortion of the deformation field due to the presence of the FWZ

As first step in our analysis, we evaluate how the presence of the FWZ affects the deformation field induced by the main pressure source active during the period under study (Fig. 1; Bonforte et al., 2008; Palano et al., 2008). As stated in the previous section, we account for the elastic properties of the local medium using the available data from previous tomography studies (Aloisi et al., 2002; Patanè et al., 2006) and simulate the presence of the FWZ by imposing, in the portion of FEM domain supposed to contain it, a lower value of E than would be expected (Fig. 3).

Relying on past studies (Bonforte et al., 2008; Palano et al., 2008; Aloisi et al., 2011; Bruno et al., 2012), the pressure source beneath the western flank of Etna is assumed to (i) be spherical (radius = 250 m), (ii) be located at a depth of 7 km b.s.l and (iii) generate an overpressure of 7 GPa. The ground deformation produced by this test source matches

the ground deformation observed during the 1993–1997 period (Palano et al., 2008), when most of the first gravity increase/decrease cycle occurred (Fig. 2b–c) — a fact that supports our model setup.

Fig. 4 shows the deformation field induced by the pressure source and calculated through the FEM numerical scheme, along a cross section (trace shown as a dashed blue line in Fig. 1) perpendicular to the FWZ. The deformation field indicated by red arrows is calculated using a lower E of 10 GPa in the portion of FEM domain containing the NNW–SSE FWZ. Black arrows indicate the results obtained without considering an "anomalous" Young's modulus across the FWZ (i.e., values of E that are interpolated from the available tomography data throughout the entire FEM domain). The presence of the FWZ causes a distortion of the deformation field that is induced by the pressure source, as indicated by the discrepancy between the two sets of vectors (Fig. 4). The same result is obtained if other values of Young's modulus are assumed (we used values of E = 5, 10, 15 and 25 GPa; Section 3.2.), provided that they are lower than the values deduced from interpolation of the available tomography data. As E approaches the higher end of the chosen range (25 GPa), the distortion of the deformation field induced by the pressure source around the FWZ becomes progressively less significant. To highlight this effect, we compute the vector difference between the deformation fields induced by the pressure source both with and without a lower value of E in correspondence of the FWZ. Results for the case where E in the FWZ is assumed to be 10 GPa are shown in Fig. 5. This figure thus presents the vector difference between the deformation fields indicated through red and black arrows, respectively, in Fig. 4. The vector difference is reported in plan view from 3 km b.s.l. — a depth that roughly coincides with the depth of the mass center of the FWZ, as deduced from gravity studies (Carbone et al., 2003a, 2009). The main feature that emerges from the vector difference is a tendency for local extension across the FWZ (Fig. 5). This result is in agreement with the hypothesized cause–effect relationship between pressurization below the western flank and the mechanical response of the medium accommodated along the FWZ (Carbone et al., 2009). The tensile dislocation across the FWZ deduced from the above vector difference is inversely proportional to the value of E assumed in the FWZ. However, even at the lower edge of the assumed range of E values (5 GPa; Section 3.2.), the calculated dislocation is much smaller than needed to induce the observed gravity changes via changes in the local rate of microfracturing (see Section 2). This discrepancy means that, for the observed gravity changes to develop via the hypothesized mechanism, an independent process must have superimposed on the mechanical response of the medium beneath the SE flank, increasing the tensile dislocation towards the needed values.

4.2. Surface deformation

Another unresolved point concerning the hypothesis of Carbone et al. (2009) is the amount of ground deformation associated with extension across the FWZ. As stated above (Section 2), analytical models based on the half-space assumption (Okubo and Watanabe, 1989) predict that a larger ground deformation than observed should have been occurred during the development of the observed gravity changes, if they were due to changes in the rate of micro-fracturing of the medium. Nevertheless, this prediction could be biased by the assumption of a mechanically homogeneous medium (Carbone et al., 2007). To address this issue, we use again the FEM approach (Section 3.1). Following our assumptions about the different mechanical characteristics of the volume containing the FWZ (Section 3.2.), we investigate how its presence influences the stress–strain behavior in the computational domain. To evaluate the amount of extension at depth, we assume the presence of a discontinuity embedded in the volume that approximates the FWZ (Figs. 1 and 3). This is a first-order assumption and may not be the most suitable to evaluate the amount of extension across the FWZ; however, any other alternatives (e.g. many small discontinuities uniformly distributed in the inferred volume) would be difficult to implement using the FEM. Rather than precisely describe the mechanical behaviors of the medium, we aim to explore the extension across the FWZ and we reason that our assumption is appropriate for this purpose.

Tensile stresses are applied across the FWZ to approximate the above cited process that controls extension across it (Section 4.1).

We perform different calculations, assuming different values for (i) the Young's modulus (assumed range of 5–25 GPa; Section 3.2) of the FWZ (values of E interpolated from the available tomography data are imposed in the rest of the computational domain) and (ii) the tensile stress applied across it. Results indicate that, when a lower value of E is assumed in the volume containing the FWZ, more extension can be accommodated at depth, for almost the same amount of deformation at the surface (Fig. 6). For example (Fig. 7), if a constant tensile stress of less than 7 MPa is applied across the FWZ, the maximum extension at depth varies by a factor of about 6 (from less than 40 cm to more than 200 cm for the cases of no anomalous E and E = 5 GPa across the FWZ, respectively), while the corresponding maximum vertical and horizontal ground deformations vary by a factor of up to only 1.2. As shown in Fig. 8, an extension of 120 cm at depth implies maximum vertical and horizontal ground deformation of 3.3 and 3.9 cm for the case of no anomalous E and of 0.7 and 0.8 cm for the case of E = 5 GPa in the FWZ. Obviously, to reach the same amount of extension at depth,

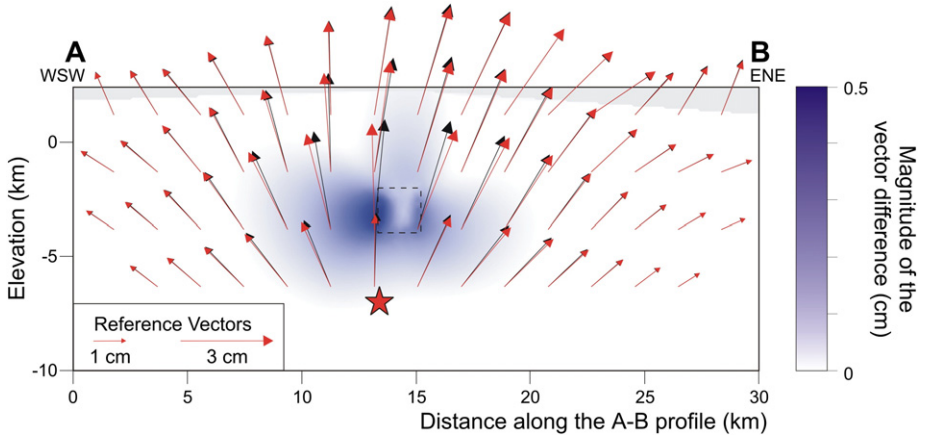

Fig. 4. Cross section along the A–B profiles in Fig. 1. The arrows (calculated through the FEM numerical scheme) represent the projected deformation fields produced by increased pressure (7 GPa) in a spherical magma chamber at 7 km b.s.l. (projected position marked by red star). Black arrows: deformation field calculated by accounting for the elastic properties of the medium, as interpolated from the available tomography data. Red arrow: deformation field calculated as before, but assuming a lower Young's modulus of 10 GPa in the FWZ (its position is marked by a dashed line).

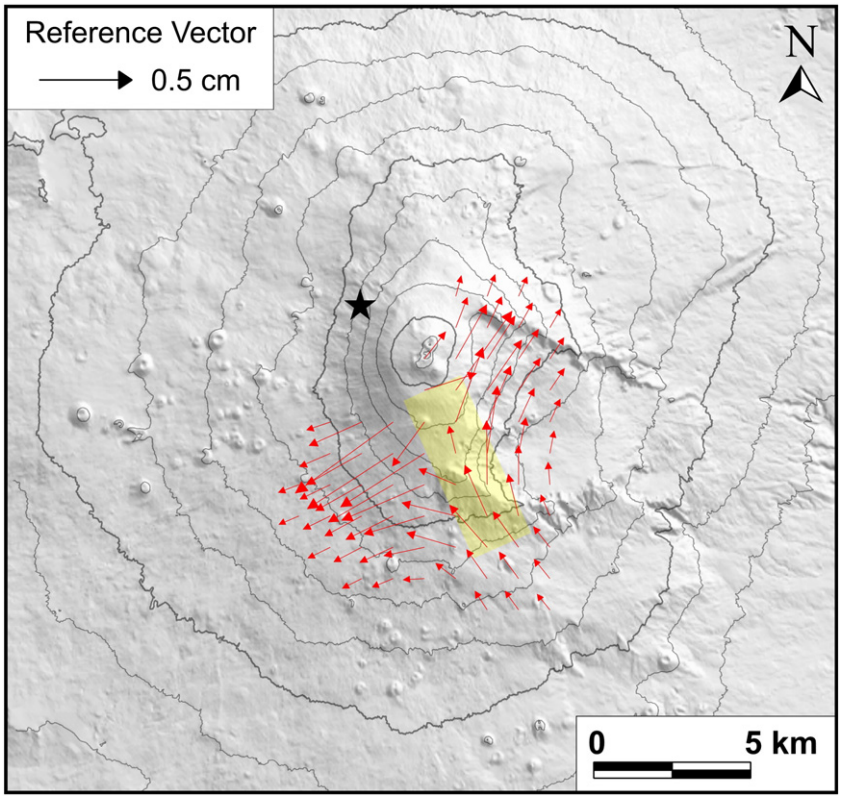

Fig. 5. Magnitude of the vector difference between the deformation fields represented by red and black arrows in Fig. 4. The vector difference is reported in plan view from 3 km b.s.l.

different tensional stresses must be applied across the FWZ when different values of E are assumed (Fig. 8).

The results presented in this section suggest that, through the assumption of a high level of damage (i.e., a lower value of E) along the FWZ, it is possible to address the issue in the interpretation of Carbone et al. (2009) regarding the relatively small ground deformation associated with the inferred deep extension (volume change). Specifically, the amount of extension across the FWZ needed to explain the observed gravity changes can be attained with negligible associated ground deformation if a value of E equal to or lower than about 10 GPa is assumed (Fig. 6).

5. Discussion of the results

Results of the numerical calculations described in the previous sections provide quantitative support for the hypothesis that the coupled gravity and strain release changes, observed at Etna during the 1994–2001 period (Carbone et al., 2009; Fig. 2), may reflect changes

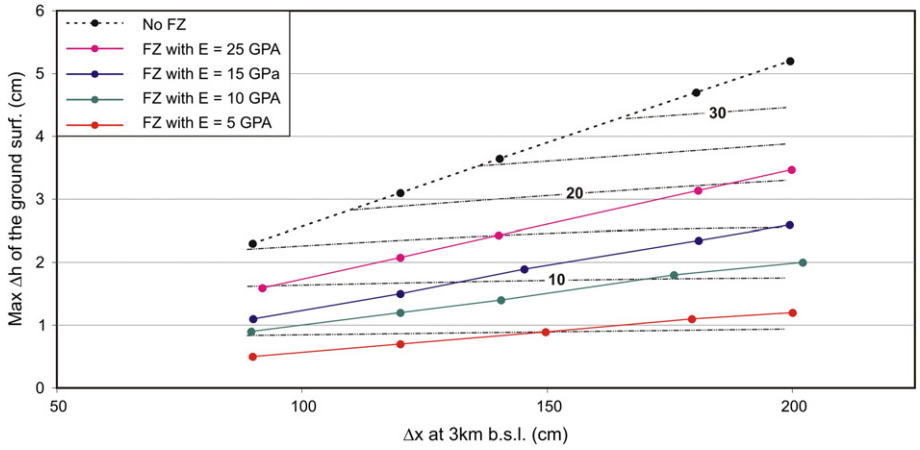

Fig. 6. Maximum vertical ground deformation versus amount of extension across the FWZ (3 km b.s.l.). The different points are calculated for different values of (i) tensile stress across the FWZ and (ii) E within the volume containing the FWZ (points with the same color refer to the same value of E). Values of E interpolated from the available tomography data are imposed in the rest of the computational domain during each calculation. Note that the black points are calculated without imposing an "anomalous" value of E within the volume containing the FWZ. The solid lines connecting the data points have no physical meaning and are drawn only to guide the eye. The dashed lines show approximate contours (in MPa) of the tensile stress applied across the FWZ.

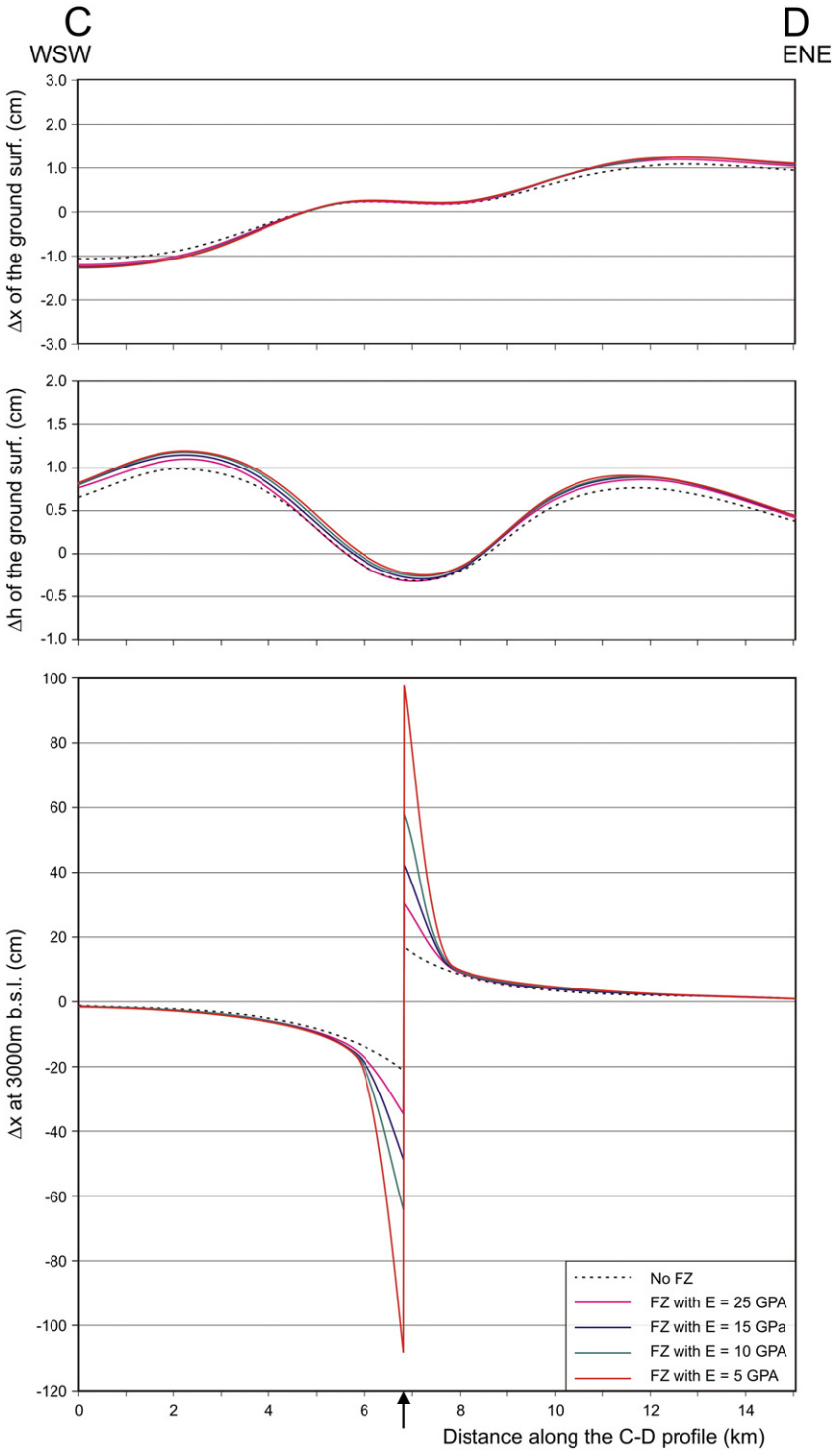

Fig. 7. Horizontal (top panel; positive towards ENE) and vertical (middle panel; positive values indicate inflation) ground displacements calculated through the FEM numerical scheme along the C–D profile of Fig. 1. Ground displacements are calculated assuming (i) a constant tensile stress of 6.8 MPa across the FWZ and (ii) different values of E within the volume containing the FWZ. The elastic properties of the medium, as deduced from the available tomography data, are accounted for in the rest of the FEM domain. Curves in the lower panel indicate extension at depth (3 km b.s.l.) across the FWZ (positive towards ENE). Ground displacements and extension indicated through dashed black lines are calculated without imposing an "anomalous" value of E within the volume containing the FWZ. The black arrow at the bottom of the graph indicates the position of the center of the FWZ.

in the rate of microfracturing of the medium. The main findings of the simulations we performed (Section 4) can be summarized as follows:

1. if it is assumed that the fracture zone inferred to cross the SE sector of the volcano (Carbone et al., 2003a, 2009; Figs. 1 and 3) is characterized by a lower Young's modulus than the surrounding medium (Heap et al., 2010, 2013), its presence causes localized extension (Figs. 4 and 5) within the deformation field induced by the deeper pressure source under the NW sector of the volcano (Bonforte et al., 2008);
2. under the hypothesis of a lower Young's modulus in the FWZ, the important extension (volume change) across it, deduced from the analysis of gravity data (see Section 2), could have developed with small surface deformation (Figs. 6, 7 and 8).

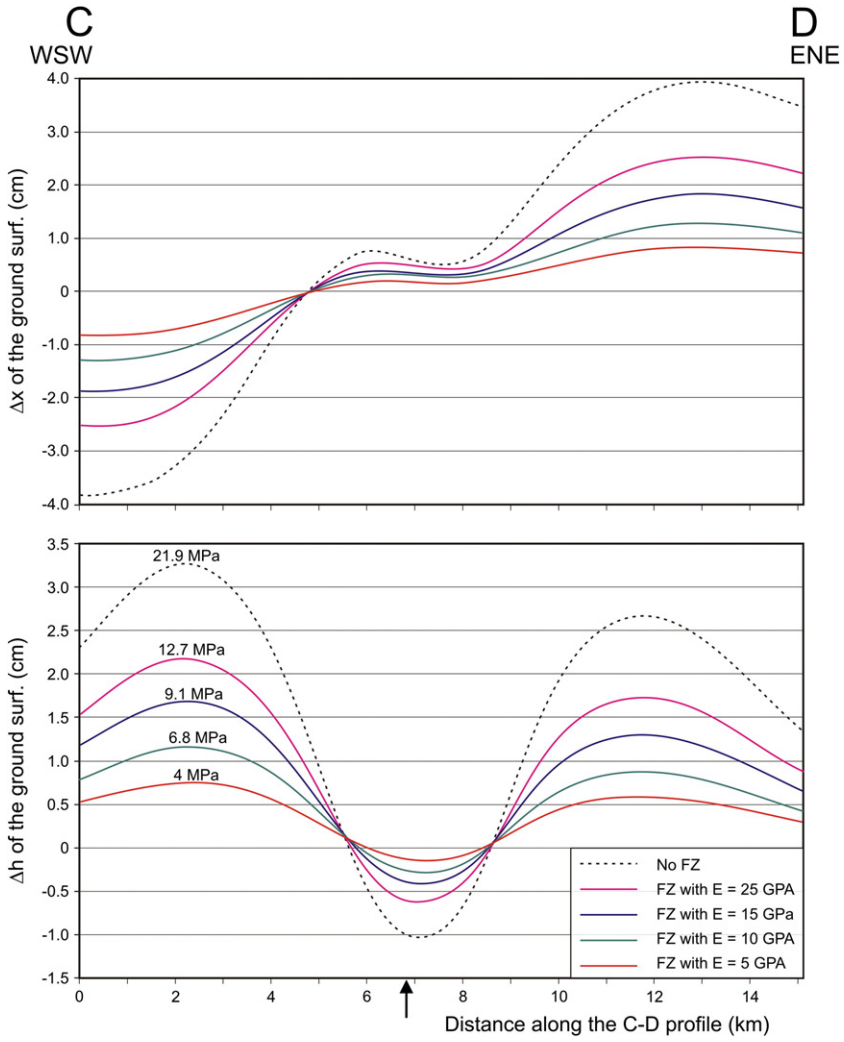

Fig. 8. Horizontal (top panel; positive towards ENE) and vertical (middle panel; positive values indicate inflation) ground displacements calculated through the FEM numerical scheme along the C–D profile of Fig. 1. Ground displacements are calculated assuming different values of (i) tensile stress across the FWZ (reported in the lower panel) and (ii) E within the volume containing the FWZ. The elastic properties of the medium, as deduced from the available tomography data, are accounted for in the rest of the FEM domain. All the exploited combinations of E and tensile stress result in a fixed amount of extension across the FWZ of about 120 cm. Ground displacements indicated through dashed black lines are calculated without imposing an "anomalous" value of E within the volume containing the FWZ. The black arrow at the bottom of the graph indicates the position of the center of the FWZ.

As stated in Section 4.1, our results suggest that the amount of extension across the FWZ only due to pressurization of the deeper magma reservoir below the NW flank of the volcano, is far too small to induce the observed gravity changes through changes in the rate of microfracturing (Fig. 5). Hence, some additional mechanism must have acted to amplify the extension. Besides magma pressure, regional stress and/or the seaward sliding of the eastern to southern flanks of the volcano (Bonforte and Puglisi, 2003; Solaro et al., 2010; Bonforte et al., 2011) could have contributed to the local stress field during the period under study, thus influencing the response across the FWZ. However, based on the available evidence, a direct causal relation between the instability-controlled flank sliding and the medium fracturing responsible for the 1994–2001 gravity changes does not seem to exist. Indeed, during the studied period, the direction of the flank motion in the area where the strongest gravity changes were observed (upper southeastern flank) was almost parallel, rather than normal, to the orientation of the FWZ (Bonaccorso et al., 2006; Bonforte et al., 2011), implying that a negligible tensile component across the FWZ was produced by the flank motion. Furthermore, there is a general lack of correspondence between the 1994–2001 phases of gravity decrease (increase of medium fracturing) and the velocity of the seaward sliding of the eastern to southern flanks (Palano et al., 2008) and, for about 5 years after the 2001 eruption, significant long-period mass changes did not occur below the southeastern flank of Etna (Carbone et al., 2009), in spite of the marked acceleration of the flank motion (Bonaccorso et al., 2006; Bonforte et al., 2008).

Another candidate mechanism for amplifying the extension across the FWZ during 1994–2001 is the establishment of a feedback loop involving local extension and the propagation of pressurized gas. Indeed, the tensile stresses induced across the FWZ by the dynamics of the deeper pressure source could have enhanced the flux of pressurized gas that, in turn, increased the extensional strain. Various authors have demonstrated that the propagation of pressurized gas may effectively generate local stress in the crust (e.g. Giammanco et al., 2008) and trigger earthquakes (Miller et al., 2004).

Our calculations (Section 4.2) indicate that a tensile stress of around 4 to 7 MPa (E up to 10 GPa along the FWZ) must be applied across the FWZ to generate significant extension, while keeping ground deformation to minimal levels (Fig. 6). The low value of E implied by our results suggests that the FWZ cuts mainly through sedimentary rocks (Section 3.2). During magma ascent above the gas-exsolution limit, gas pressure may exceed ambient pressure by up to several MPa, because of the hindering effect on the expansion of bubbles (Gonnermann and Manga, 2013; Mueller et al., 2013). This effect is mainly driven by magma viscosity

that is, in turn, controlled by volatile exsolution and adiabatic cooling. At shallower depths, most of the outgassing from the magma is thought to occur along an interconnected pore-fracture network within the magma body (permeable outgassing; Edmonds et al., 2003). Below the level where the pathway of cracks and bubbles is established, gas may escape from the magma through the wall rock, provided that it is permeable and at a lower ambient pressure than the gas pressure. However, the extent to which degassing into wall rocks occurs in nature is a matter of debate (Boudon et al., 1998; Gonnermann and Manga, 2013). According to Norton (1990), in the near-field regions of magma bodies, changes in fluid pressure occur during the dissipation of thermal energy, resulting in large local stresses and the formation and growth of fracture networks on either side of the pluton, which facilitate fluid flow.

Soil gas emissions from the lower flanks of Etna indicate that gas flux does occur through peripheral sectors of the volcano (Gurrieri et al., 2008). In particular, Federico et al. (2011) showed that during the period between the 1991–93 and 2001 main flank eruptions, the rate of soil CO_2 efflux from the lower southern flank of Etna was higher than the average. This evidence supports the hypothesis that the passage of pressurized gas could have contributed to the inferred changes of fracturing rate along the FWZ.

It is worth noting that other processes, such as crack growth (that can occur even under compressive stresses; Heap et al., 2009, 2010) and thermally-induced decarbonation (Mollo et al., 2012), could have contributed to the development of the 1996–1999 and 2000–2001 phases of gravity decrease (Fig. 2c, d, f).

Changes in the sign of the slope of the coupled gravity/strain release curves during 1994–2001 (Fig. 2) could have resulted from competitive interactions between different mechanisms, including flux of overpressurized gas (in turn modulated by the intrusion of new undegassed magma into the upper feeding system; Gurrieri et al., 2008) and gravitational loading of the volcanic edifice (Aloisi et al., 2011). As a result, depending on whether the rate of microfracturing in the FWZ increased or decreased, phases of gravity decrease or increase, respectively, developed.

Despite the inherent limitations, the results of the present study provide an opportunity to address the mismatch between sources of pressure and mass changes that were active at Etna between 1994 and 2001. A lower-than-expected Young's modulus in the FWZ may allow a large amount of extension across it (thus gravity changes driven by changes in the rate of medium fracturing), accompanied by small surface deformation (Fig. 6). The latter would be difficult to detect also because it would be swamped by the effect of the pressure source below the western flank of the volcano. The vertical displacement fields induced by (i) increased pressure (7 GPa) in a spherical magma chamber below the west flank of the volcano (7 km b.s.l.) and (ii) the same pressure source plus tensile stresses (6.8 MPa) across the FWZ (2–4 km b.s.l.), both calculated using FEM, are presented in panels a and b, respectively, of Fig. 9. In both calculations we account for the elastic properties of the medium, as deduced from the available tomography data, and set E in the FWZ to a value of 10 GPa. Despite the considerable amount of extension across the FWZ (larger than 1 m), the applied tensile stresses result only in a small perturbation of the vertical ground deformation induced by the deeper pressure source (in the order of +/− 1 cm; panels c and d of Fig. 9). This perturbation would be difficult to recognize through analysis of GPS data (whose uncertainty is close to 1 cm; Palano et al., 2008). It is worth stressing that ground motion data obtained through the Permanent Scatterer InSAR technique (Bonforte et al., 2011) during 1995–2000 do suggest a deformation pattern in the upper southwestern flank similar to the simulated one (Fig. 9b).

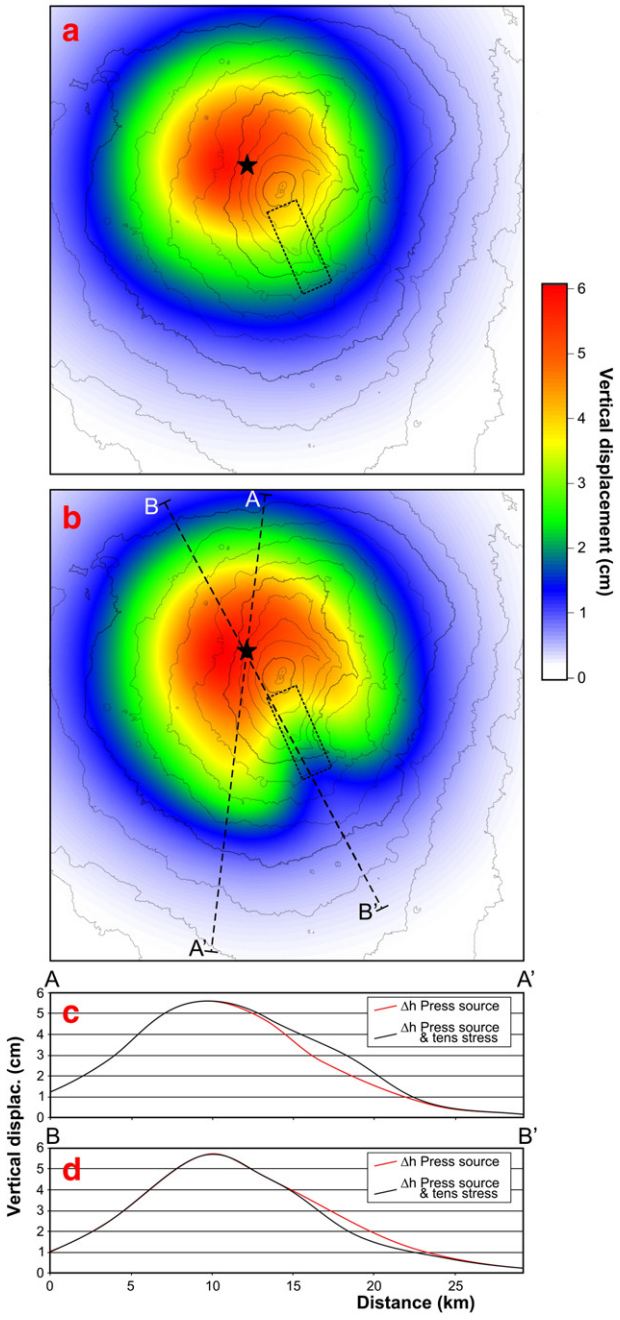

Fig. 9. (a) Vertical ground displacement produced by increased pressure (7 GPa) in a spherical magma chamber at 7 km b.s.l., whose surface projection is marked through a black star. (b) Same as (a), but also considering tensile dislocation of 120 cm across the FWZ, where an anomalous value of E (10 GPa) is assumed (tensile stress acting across the FWZ = 6.8 MPa). (c) Cross section along the A–A′ trace showing comparison between ground displacements reported in (a) and (b). (d) Cross section along the B–B′ trace showing comparison between ground displacements reported in (a) and (b). The elastic properties of the medium, as deduced from the available tomography data, are accounted for over the whole domain, except for the volume containing the FWZ.

6. Conclusions

At Mt. Etna the complex interplay between magma dynamics and the thermomechanical response of the host medium may influence the mechanisms of magma transport, thus exerting control on the eruptive activity (Aloisi et al., 2011; Privitera et al., 2012). As a consequence, the temporal variation of geophysical and geochemical parameters monitored at the surface may be different from that expected when simple models of magma transport are applied. A deeper understanding of the causal linkages thus requires improved monitoring systems, involving as many parameters as possible, and advanced modeling methods.

During the time interval between the 1991–93 and 2001 flank eruptions, volcanic activity was confined to the summit vents (Allard et al.,

2006; Behncke et al., 2006). Ground deformation and tomography studies (Chiarabba et al., 2000; Bonforte et al., 2008; Palano et al., 2008) suggest that this activity was driven by a magma body located beneath the northwest flank of the volcano, at a depth of about 7 km (Figs. 1 and 10). Gravity studies (Budetta et al., 1999; Carbone et al., 2003a, 2003b), however, indicate that the most important mass redistributions during the same period took place at shallower depth below the southeastern sector of the volcano (Figs. 1 and 10). The late-1996 to mid-1999 and late-2000 to mid-2001 phases of gravity decrease coincide with phases of higher strain release rate (bottom graph of Fig. 2) and seismicity at 2–4 km depth, clusters within the volume inferred to contain the gravity source (panels c, d and f of Fig. 2). Carbone et al. (2009) proposed that the coupling between gravity and seismic data reflects changes in the rate of micro-fracturing along the NNW–SSE-oriented fracture/weakness zone (FWZ) that underlies the SE slope of the volcano. This interpretation explains the difference in locations of the pressure and mass sources active at Etna during 1994–2001 (Fig. 10).

The 1996–99 and 2000–01 phases of gravity decrease/strain release increase would thus image phases of increase in the rate of micro-fracturing along the FWZ. This process could eventually lead to the formation of a magma ascent path to the surface through mechanical failure of the rocks above the storage area (Cosgrove, 1997; Scandone et al., 2007). The 1996–99 phase of increasing fracturing did not lead to a flank eruption. The overall negative trend of gravity during this period (panels c and d in Fig. 2) suggests that, if a density increase was actually produced by a lateral intrusion, it was not enough to counteract the decrease due to the ongoing fracturing of the medium. However, the discrepancy between gravity and strain release curves for about one year after January 1998 (bottom graph in Fig. 2; see Section 2) may represent the gravity signature of the shallow magma intrusion inferred by Bonaccorso and Patanè (2001).

The subsequent phase of increase in the rate of micro-fracturing (late-2000 to mid-2001; Fig. 2f) allowed the fast magma ascent (Pompilio et al., 2001; Corsaro et al., 2007) that eventually led to the 2001 eruption. In agreement with this scenario, a sudden gravity increase occurred soon after the start of the eruption, indicating that magma was emplaced along the FWZ, partially compensating the previous negative variation (Carbone et al., 2003b).

For 5 years after the end of the 2001 eruption, significant long-period mass changes did not occur below the southeastern flank of Etna (Carbone et al., 2009), as a consequence of the structural modification in the shallow plumbing system (Allard et al., 2006; Carbone et al., 2009) that also affected the long-term pressure buildup in the deeper western pressure source. Indeed, since the beginning of the new eruptive phase marked by the 2001 eruption, the trend of the dilatation of the western part of the volcano markedly decelerated, while the dilatation of the whole volcano continued, mainly driven by accelerated flank instability (Neri et al., 2005; Bonaccorso et al., 2006; Bonforte et al.,

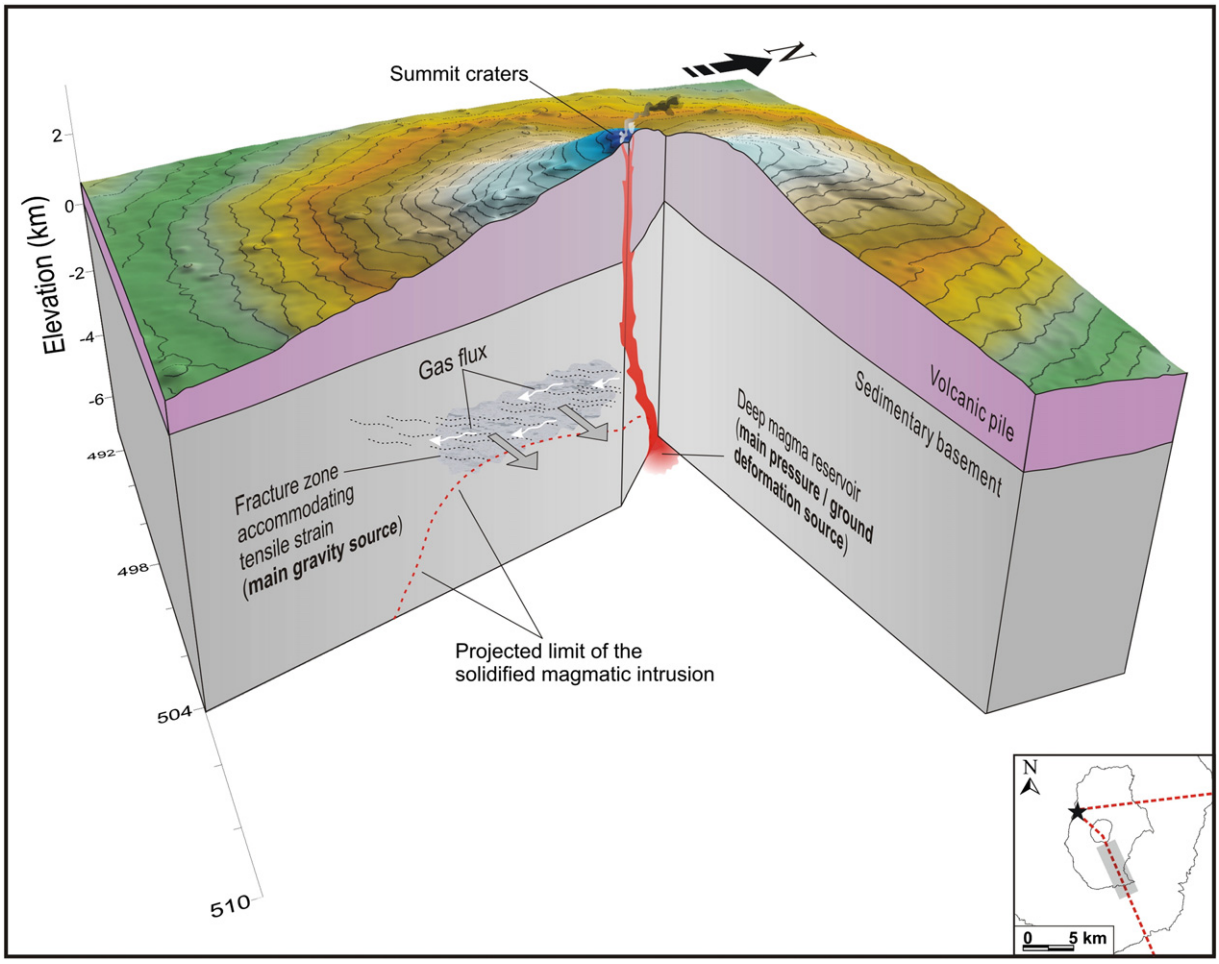

Fig. 10. 3-D representation demonstrating our model for processes that occurred at Etna during 1994–2001. During that interval, volcanic activity was confined to the summit craters and fed by a reservoir below the western flank of the volcano (star in Fig. 1). The latter was inferred to be the main source of ground deformation during the period (e.g. Bonforte et al., 2008). The FWZ below the SE sector of the volcano, inferred to be the most important source of gravity changes during 1994–2001 (e.g. Carbone et al., 2009), is peripheral to the region of magma ascent from the deep storage area to the surface. Tensile stresses acting across the FWZ (gray arrows) induced changes in the rate of microfracturing that, in turn, caused the local gravity changes observed at the surface. These tensile stresses could have been enhanced by propagation of pressurized gas (white arrows). The projected limit of the solidified magmatic intrusion (mainly developed to the E of the FWZ) is averaged from different tomography studies. The bottom-right inset indicates (i) the surface trace of the 3D cross-section, (ii) the surface projection of the FWZ (gray box) and (iii) the surface projection of the deeper pressure source (black star).

2008). These observations suggest that, while the 1994–2001 gravity changes observed in the southeastern sector of Etna were somehow related to the pressure source below the western flank of the volcano, there is not a direct causal link with the instability of the eastern to southern flanks.

Carbone et al. (2009) suggested that the inferred 1994–2001 extensional dynamics of the southeastern flank of Etna may represent a second-order effect, triggered by the pressure source below the west flank and accommodated along the NNW–SSE FWZ.

To gain quantitative insight into the relations between stress, strain and mass changes at Etna during 1994–2001, we use the FEM modeling approach. Relying on recent studies involving stress- and temperature-induced degradation of the mechanical properties of rocks (Heap et al., 2010, 2013), we hypothesize that the FWZ is characterized by an anomalously low Young's modulus. Results of our analysis indicate that:

(i) the presence of the FWZ creates a distortion of the displacement field induced by the deeper pressure source, locally resulting in a weak extensional regime (Section 4.1; Figs. 4 and 5);
(ii) for a given tensile stress across the FWZ, the amount of extension at depth increases proportionally as the value of Young's modulus in the FWZ decreases, while the ground deformation remains almost the same (Section 4.2; Figs. 6 and 7).

The finding summarized in (i) lends support to the hypothesis of a cause–effect relation between deeper pressurization beneath the western flank and shallower extension across the FWZ beneath the SE flank of the volcano (Carbone et al., 2009). However, the extension across the FWZ due solely to pressurization of the magma reservoir (Fig. 5) is not sufficient to induce the observed gravity changes through variations in the rate of microfracturing. We suggest that propagation of pressurized gas may have enhanced tensile stresses across the FWZ (Miller et al., 2004), in turn increasing the amount of extension (Fig. 10).

The finding summarized in (ii) furnishes a valuable key to understanding how, during the studied period, the inferred changes in the bulk rate of microfracturing along the FWZ could have occurred without significant variations in ground deformation. Indeed, we find that, as the value of Young's modulus in the FWZ decreases, the ratio between the amount of extension at depth and the maximum ground displacement increases (Figs. 7 and 8) and, for values of Young's modulus that are equal or less than about 10 GPa, deep extension of 1–2 m can develop with deformation of the surface that is close to the detection limit of GPS measurements (Fig. 6).

Past studies have shown that residual gravity changes not accompanied by significant ground displacement may occur due to magma intrusion into void spaces (Rymer et al., 1993; Johnson et al., 2010) or changes in the average density of shallow magma bodies (Eggers, 1987; Battaglia et al., 2008). Here we provide quantitative support to the hypothesis that gravity studies may also illuminate changes in the fracturing rate of "dry" portions of the medium, even when they take place with negligible displacement of the ground surface. The importance of detecting these changes is demonstrated by the fact that, during a phase of increasing fracturing rate, the FWZ was used as a path for magma flow to the surface soon before the onset of the Etna's 2001 eruption (Carbone et al., 2003a, 2009; Puglisi et al., 2008).

Our results therefore emphasize the importance of integrating the most common volcano monitoring techniques with gravity studies. Indeed, they may be of crucial importance for eruption forecasting at volcanoes where there is a causal link between medium fracturing and volcanic activity, for example, at Etna (Carbone et al., 2009), Piton de la Fournaise (Brenguier et al., 2008) and Soufrière Hills Volcano (Hautmann et al., 2010).

Acknowledgments

This work was financed through the project "MED-SUV" that received funding from the European Union's Seventh Programme for research, technological development and demonstration under grant agreement No 308665. The final version of the paper benefited from comments by M. P. Poland and another anonymous reviewer.

References

Allard, P., 1997. Endogenous magma degassing and storage at Mount Etna. Geophys. Res. Lett. 24, 2219–2222.
Allard, P., Behncke, B., D'Amico, S., Neri, M., Gambino, S., 2006. Mount Etna 1993–2005: anatomy of an evolving eruptive cycle. Earth Sci. Rev. 78, 85–114. http://dx.doi.org/10.1016/j.earscirev. 2006.04.002.
Aloisi, M., Cocina, O., Neri, G., Orecchio, B., Privitera, E., 2002. Seismic tomography of the crust underneath the Etna volcano, Sicily. Phys. Earth Planet. Inter. 134, 139–155. http://dx.doi.org/10.1016/S0031-9201(02)00153-X.
Aloisi, M., Mattia, M., Monaco, C., Pulvirenti, F., 2011. Magma, faults, and gravitational loading at Mount Etna: the 2002–2003 eruptive period. J. Geophys. Res. 116. http://dx.doi.org/10.1029/2010 JB007909 B05203.
Alparone, S., Andronico, D., Lodato, L., Sgroi, T., 2003. Relationship between tremor and volcanic activity during the Southeast Crater eruption on Mount Etna in early 2000. J. Geophys. Res. 108. http://dx.doi.org/10.1029/2002JB001866.
Andronico, D., Branca, S., Calvari, S., Burton, M., Caltabiano, T., Corsaro, R.A., Del Carlo, P., Garfì, G., Lodato, L., Miraglia, L., Murè, F., Neri, M., Pecora, E., Pompilio, M., Salerno, G., Spampinato, L., 2005. A multi-disciplinary study of the 2002–03 Etna eruption: insights into a complex plumbing system. Bull. Volcanol. 67, 314–330. http://dx.doi.org/10.1007/s00445-004-0372-8.
Battaglia, M., Segall, P., Roberts, C., 2003. The mechanics of unrest at Long Valley caldera, California. 2. Constraining the nature of the source using geodetic and microgravity data. J. Volcanol. Geotherm. Res. 127 (3–4), 219–245.
Battaglia, M., Gottsmann, J., Carbone, D., Fernández, J., 2008. 4D volcano gravimetry. Geophysics 73 (6). http://dx.doi.org/10.1190/1.2977792.
Behncke, B., Neri, M., 2003. Cycles and trends in the recent eruptive behaviour of Mt. Etna (Italy). Can. J. Earth Sci. 40, 1405–1411. http://dx.doi.org/10.1139/E03-052.
Behncke, B., Neri, M., Pecora, E., Zanon, V., 2006. The exceptional activity and growth of Southeast Crater, Mount Etna (Italy), between 1996 and 2001. Bull. Volcanol. 69. http://dx.doi.org/10.1007/s00445-006-0061-x.
Blake, S., 1981. Volcanism and the dynamics of open magma chambers. Nature 289, 783–785. http://dx.doi.org/10.1038/289783a0.
Bonaccorso, A., Patanè, D., 2001. Shear response to an intrusive episode at Mt. Etna Volcano (January 1998) inferred through seismic and tilt data. Tectonophysics 334, 61–75.
Bonaccorso, A., Bonforte, A., Guglielmino, F., Palano, M., Puglisi, G., 2006. Composite ground deformation pattern forerunning the 2004–2005 Mount Etna eruption. J. Geophys. Res. 111, B12207. http://dx.doi.org/10.1029/2005JB004206.
Bonaccorso, A., Bonforte, A., Currenti, G., Del Negro, C., Di Stefano, A., Greco, F., 2011. Magma storage, eruptive activity and flank instability: inferences from ground deformation and gravity changes during the 1993–2000 recharging of Mt. Etna volcano. J. Volcanol. Geotherm. Res. http://dx.doi.org/10.1016/j.jvolgeores.2011.01.001.
Bonforte, A., Puglisi, G., 2003. Magma uprising and flank dynamics on Mount Etna volcano, studied using GPS data (1994–1995). J. Geophys. Res. 108 (B3), 2153. http://dx.doi.org/10.1029/2002J B001845.
Bonforte, A., Puglisi, G., 2006. Dynamics of the eastern flank of Mt Etna volcano (Italy) investigated by a dense GPS network. J. Volcanol. Geotherm. Res. 153, 357–369. http://dx.doi.org/10.1016/j.jvolgeores.2005.12.005.
Bonforte, A., Bonaccorso, A., Guglielmino, F., Palano, M., Puglisi, G., 2008. Feeding system and magma storage beneath Mt Etna as revealed by recent inflation/deflation cycles. J. Geophys. Res. Solid Earth 113, B05456. http://dx.doi.org/10.1029/2007JB005334.
Bonforte, A., Guglielmino, F., Coltelli, M., Ferretti, A., Puglisi, G., 2011. Structural assessment of Mount Etna volcano from Permanent Scatterers analysis. Geochem. Geophys. Geosyst. 12, Q02002. http://dx.doi.org/10.1029/2010GC003213.
Bonvalot, S., Remy, D., Deplus, C., Diament, M., Gabalda, G., 2008. Insights on the March 1998 eruption at Piton de la Fournaise volcano (La Re´union) from microgravity monitoring. J. Geophys. Res. 113, B05407. http://dx.doi.org/10.1029/2007JB005084.
Boudon, G., Villemant, B., Komorowski, J.C., Ildefonse, P., Semet, M.P., 1998. The hydrothermal system at Soufriere Hills volcano, Montserrat (West Indies): characterization and role in the on-going eruption. Geophys. Res. Lett. 25, 3693–3696.
Bousquet, J.C., Lanzafame, G., 2004. The tectonics and geodynamics of Mount Etna: synthesis and interpretation of geological and geophysical data. In: Bonaccorso, A., et al. (Eds.), Etna Volcano Laboratory, Geophys. Monogr. Ser, vol. 143. AGU, Washington, D.C., pp. 29–47.
Branca, S., Carbone, D., Greco, F., 2003. Intrusive mechanism of the 2002 NE-Rift eruption at Mt. Etna (Italy) inferred through continuous microgravity data and volcanological evidences. Geophys. Res. Lett. 30, 2077. http://dx.doi.org/10.1029/2003GL018250.
Brenguier, F., Shapiro, N.M., Campillo, M., Ferrazzini, V., Duputel, Z., Coutant, O., Nercessian, A., 2008. Towards forecasting volcanic eruptions using seismic noise. Nat. Geosci. 1, 126–130. http://dx.doi.org/10.1038/ngeo104.
Bruno, V., Mattia, M., Aloisi, M., Palano, M., Cannavò, F., Holt, W.E., 2012. Ground deformations and volcanic processes as imaged by CGPS data at Mt. Etna (Italy) between 2003 and 2008. J. Geophys. Res. Solid Earth 117, B07208. http://dx.doi.org/10.1029/2011JB009114.
Budetta, G., Carbone, D., Greco, F., 1999. Subsurface mass redistribution at Mount Etna (Italy) during the 1995–1996 explosive activity detected by microgravity studies. Geophys. J. Int. 138, 7–88.
Calvari, S., Coltelli, M., Neri, M., Pompilio, M., Scribano, V., 1994. The 1991–1993 Etna eruption: chronology and lava flow-field evolution. Acta Vulcanol. 4, 1–14.

Carbone, D., Budetta, G., Greco, F., 2003a. Bulk processes prior to the 2001 Mount Etna eruption, highlighted through microgravity studies. J. Geophys. Res. 108, 2556. http://dx.doi.org/10.1029/2003JB002542.
Carbone, D., Budetta, G., Greco, F., 2003b. Possible mechanisms of magma redistribution under Mt Etna during the 1994–1999 period detected through microgravity measurements. Geophys. J. Int. 153, 187–200.
Carbone, D., Currenti, G., Del Negro, C., 2007. Elastic model for the gravity and elevation changes before the 2001 eruption of Etna volcano. Bull. Volcanol. 69, 553–562. http://dx.doi.org/10.1007/s00445-006-0090-5.
Carbone, D., D'Amico, S., Musumeci, C., Greco, F., 2009. Comparison between the 1994–2006 seismic and gravity data from Mt. Etna: new insight into the long-term behavior of a complex volcano. Earth Planet. Sci. Lett. 279, 282–292. http://dx.doi.org/10.1016/j.epsl.2009.01.007.
Catalano, S., Torrisi, S., Ferlito, C., 2004. The relationship between late quaternary deformation and volcanism of Mt. Etna (eastern Sicily): new evidence from the sedimentary substratum in the Catania region. J. Volcanol. Geotherm. Res. 132, 311–334.
Charco, M., Camacho, A.G., Tiampo, K.F., Fernández, J., 2009. Spatiotemporal gravity changes on volcanoes: assessing the importance of topography. Geophys. Res. Lett. 36, L08306. http://dx.doi.org/10.1029/2009GL037160.
Chiarabba, C., Amaro, A., Boschi, E., 2000. Recent seismicity and tomographic modeling of the Mount Etna plumbing system. J. Geophys. Res. Solid Earth 105 (B5), 10,923–10,938. http://dx.doi.org/10.1029/1999JB900427.
Chiocci, F.L., Coltelli, M., Bosman, A., Cavallaro, D., 2011. Continental margin large-scale instability controlling the flank sliding of Etna volcano. Earth Planet. Sci. Lett. 305 (1–2), 57–64. http://dx.doi.org/10.1016/j.epsl.2011.02.040.
Cianetti, S., Giunchi, C., Casarotti, E., 2012. Volcanic deformation and flank instability due to magmatic sources and frictional rheology: the case of Mount Etna. Geophys. J. Int. 191 (3), 939–953. http://dx.doi.org/10.1111/j.1365-246X.2012.05689.x.
Corsaro, R.A., Miraglia, L., Pompilio, M., 2007. Petrologic evidence of a complex plumbing system feeding the July–August 2001 eruption of Mt. Etna, Sicily, Italy. Bull. Volcanol. 69, 401–421. http://dx.doi.org/10.1007/s00445-006-0083-4.
Cosgrove, J.W., 1997. The influence of mechanical anisotropy on the behaviour of the lower crust. Tectonophysics 280 (1), 1–14.
De Gori, P., Chiarabba, C., Patanè, D., 2005. Qp structure of Mount Etna: constraints for the physics of the plumbing system. J. Geophys. Res. 110, 0B05303. http://dx.doi.org/10.1029/2003JB002875.
Edmonds, M., Oppenheimer, C., Pyle, D.M., Herd, R.A., Thompson, G., 2003. SO_2 emissions from Soufriere Hills Volcano and their relationship to conduit permeability, hydrothermal interaction and degassing regime. J. Volcanol. Geotherm. Res. 124, 23–43.
Eggers, A.A., 1987. Residual gravity changes and eruption magnitudes. J. Volcanol. Geotherm. Res. 33, 201–216.
Falsaperla, S., Cara, F., Rovelli, A., Neri, M., Behncke, B., Acocella, V., 2010. Effects of the 1989 fracture system in the dynamics of the upper SE flank of Etna revealed by volcanic tremor data: the missing link? J. Geophys. Res. 115, B11306. http://dx.doi.org/10.1029/2010JB007529.
Famin, V., Michon, L., 2010. Volcano destabilization by magma injections in a detachment. Geology 38 (3), 219–222. http://dx.doi.org/10.1130/G30717.1.
Federico, C., Camarda, M., De Gregorio, S., Gurrieri, S., 2011. Long-term record of CO_2 degassing along Mt. Etna's flanks and its relationship with magma dynamics and eastern flank instability. Geochem. Geophys. Geosyst. 12, Q10002. http://dx.doi.org/10.1029/2011GC003601.
Gerbault, M., Cappa, F., Hassani, R., 2012. Elasto-plastic and hydromechanical models of failure around an infinitely long magma chamber. Geochem. Geophys. Geosyst. 13, Q03009. http://dx.doi.org/10.1029/2011GC003917.
Giammanco, S., Palano, M., Scaltrito, A., Scarfì, L., Sortino, F., 2008. Possible role of fluid overpressure in the generation of earthquake swarms in active tectonic areas: the case of the Peloritani Mts. (Sicily, Italy). J. Volcanol. Geotherm. Res. 178, 795–806. http://dx.doi.org/10.1016/j.jvolgeores.2008.09.005.
Gonnermann, H.M., Manga, M., 2013. Dynamics of magma ascent in the volcanic conduit. In: Fagents, S.A., Gregg, T.K.P., Lopes, R.M.C. (Eds.), Modeling Volcanic Processes, The Physics and Mathematics of Volcanism. Cambridge University Press, pp. 55–84.
Grasso, M., Lentini, F., 1982. Sedimentary and tectonic evolution of the eastern Hyblean Plateau (southeastern Sicily) during late Cretaceous to Quaternary time. Palaeogeogr. Palaeoclimatol. Palaeoecol. 39, 261–280.
Greco, F., Currenti, G., Del Negro, C., Napoli, R., Budetta, G., Fedi, M., Boschi, E., 2010. Spatio-temporal gravity variations to look deep into the southern flank of Etna volcano. J. Geophys. Res. 115, B11411. http://dx.doi.org/10.1029/2009JB006835.
Gurrieri, S., Liuzzo, M., Giudice, G., 2008. Continuous monitoring of soil CO_2 flux on Mt. Etna: the 2004–2005 eruption and the role of regional tectonics and volcano tectonics. J. Geophys. Res. 113, B09206. http://dx.doi.org/10.1029/2007JB005003.
Harlow, D.H., Power, J.A., Laguerta, E., Ambubuyong, G., White, R.A., Hoblitt, R.P., 1996. Precursory seismicity and forecasting of the June 15, 1991, eruption of Mount Pinatubo. In: Newhall, C.G., Punongbayan, R.S. (Eds.), Fire and Mud. Univ. of Wash. Press, Seattle, pp. 285–306.
Hautmann, S., Gottsmann, J., Sparks, R.S.J., Costa, A., Melnik, O., Voight, B., 2009. Modelling ground deformation caused by oscillating overpressure in a dyke conduit at Soufrière Hills Volcano, Montserrat. Tectonophysics 471, 87–95. http://dx.doi.org/10.1016/j.tecto.2008.10.021.
Hautmann, S., Gottsmann, J., Camacho, A.G., Fournier, N., Sacks, I.S., Sparks, R.S.J., 2010. Mass variations in response to magmatic stress changes at soufrière Hills Volcano Montserrat (W. I.): insights from 4-D gravity data. Earth Planet. Sci. Lett. 290 (1–2), 83–89. http://dx.doi.org/10.1016/j.epsl.2009.12.004.
Heap, M.J., Vinciguerra, S., Meredith, P.G., 2009. The evolution of elastic moduli with increasing crack damage during cyclic stressing of a basalt from Mt. Etna volcano. Tectonophysics 471, 153–160. http://dx.doi.org/10.1016/j.tecto.2008.10.004.
Heap, M.J., Faulkner, D.R., Meredith, P.G., Vinciguerra, S., 2010. Elastic moduli evolution and accompanying stress changes with increasing crack damage: implications for stress changes around fault zones and volcanoes during deformation. Geophys. J. Int. 183, 225–236. http://dx.doi.org/10.1111/j.1365-246X.2010.04726.x.
Heap, Y.M.J., Lavallée, Y., Laumann, A., Hess, K.-U., Meredith, P.G., Dingwell, D.B., Huismann, S., Weise, F., 2013. The influence of thermal-stressing (up to 1000 °C) on the physical, mechanical, and chemical properties of siliceous-aggregate, high-strength concrete. Constr. Build. Mater. 42, 248–265. http://dx.doi.org/10.1016/j.conbuildmat.2013.01.020.
Hirn, A., Nercessian, A., Sapin, M., Ferrucci, F., Wittlinger, G., 1991. Seismic heterogeneity of Mt Etna: structure and activity. Geophys. J. Int. 105, 139–153.
Houlié, N., Briole, P., Bonforte, A., Puglisi, G., 2006. Large scale ground deformation of Etna observed by GPS between 1994 and 2001. Geophys. Res. Lett. 33, L02309. http://dx.doi.org/10.1029/2005GL024414.
Johnson, D.J., Eggers, A.A., Bagnardi, M., Battaglia, M., Poland, M.P., Miklius, A., 2010. Shallow magma accumulation at Kilauea Volcano, Hawai'i, revealed by microgravity surveys. Geology 38, 1139–1142. http://dx.doi.org/10.1130/G31323.1.
Lentini, F., 1982. The geology of the Mt. Etna basement. Mem. Soc. Geol. It. 23, 7–25.
Linde, A.T., Agustsson, K., Sacks, I.S., Stefansson, R., 1993. Mechanism of the 1991 eruption of Hekla from continuous borehole strain monitoring. Nature 365, 737–740.
Lundgren, P., Berardino, P., Coltelli, M., Fornaro, G., Lanari, R., Puglisi, G., Sansosti, E., Tesauro, M., 2003. Coupled magma chamber inflation and sector collapse slip observed with synthetic aperture radar interferometry on Mt. Etna volcano. J. Geophys. Res. 108 (B5), 2247. http://dx.doi.org/10.1029/2001JB000657.
Lundgren, P., Casu, F., Manzo, M., Pepe, A., Berardino, P., Sansosti, E., Lanari, R., 2004. Gravity and magma induced spreading of Mount Etna volcano revealed by satellite radar interferometry. Geophys. Res. Lett. 31, L04602. http://dx.doi.org/10.1029/2003GL018736.
Malone, S.D., Boyko, C., Weaver, C.S., 1983. Seismic precursors to the Mt St Helens eruptions in 1981 and 1982. Science 221, 1376–1378.
Manconi, A., Walter, T.R., Amelung, F., 2007. Effects of mechanical layering on volcano deformation. Geophys. J. Int. 170 (2), 952–958. http://dx.doi.org/10.1111/j.1365-246X.2007.03449.x.
McTigue, D.F., 1987. Elastic stress and deformation near a finite spherical magma body: resolution of the point source paradox. J. Geophys. Res. 92, 12,931–12,940.
Michelini, A., McEvilly, T.V., 1991. Seismological studies at Parkfield. I. Simultaneous inversion for velocity structure and hypocenters using cubic B-splines parameterization. Bull. Seismol. Soc. Am. 81, 524–552.
Miller, S.A., Collettini, C., Chiaraluce, L., Cocco, M., Barchi, M., Kaus, B.J.P., 2004. Aftershocks driven by a high-pressure CO_2 source at depth. Nature 427, 724–727.
Mollo, S., Heap, M.J., Iezzi, G., Hess, K.-U., Scarlato, P., Dingwell, D.B., 2012. Volcanic edifice weakening via decarbonation: a self-limiting process? Geophys. Res. Lett. 36, L15307. http://dx.doi.org/10.1029/2012GL052613.
Mueller, S., Scheu, B., Spieler, O., Dingwell, D.B., 2013. Permeability control on magma fragmentation. Geology 36, 399–402. http://dx.doi.org/10.1130/G24605A.1.
Neri, M., Acocella, V., Behncke, B., Maiolino, V., Ursino, A., Velardita, R., 2005. Contrasting triggering mechanisms of the 2001 and 2002–2003 eruptions of Mount Etna (Italy). J. Volcanol. Geotherm. Res. 144, 235–255. http://dx.doi.org/10.1016/j.jvolgeores.2004.11.025.
Norton, D.L., 1990. Pore fluid pressure near magma chambers. The Role of Fluids in Crustal Processes. The National Academies Press, Washington DC, pp. 42–49.
Okubo, S., Watanabe, H., 1989. Gravity change caused by a fissure eruption. Geophys. Res. Lett. 16, 445–448.
Palano, M., Puglisi, G., Gresta, S., 2008. Ground deformation patterns at Mt. Etna from 1993 to 2000 from joint use of InSAR and GPS techniques. J. Volcanol. Geotherm. Res. 169, 99–120.
Patanè, D., Mattia, M., Aloisi, M., 2005. Shallow intrusive processes during 2002–2004 and current volcanic activity on Mt. Etna. Geophys. Res. Lett. 32, L06302. http://dx.doi.org/10.1029/2004GL021773.
Patanè, D., Barberi, G., Cocina, O., De Gori, P., Chiarabba, C., 2006. Time-resolved seismic tomography detects magma intrusions at Mount Etna. Science 313, 821–823.
Pedley, H.M., Grasso, M., 1992. Miocene syntectonic sedimentation along the western margins of the Hyblean-Malta platform: a guide to plate margin processes in the central Mediterranean. J. Geodyn. 79, 189–202.
Pinel, V., Jaupart, C., 2000. The effect of edifice load on magma ascent beneath a volcano. Philos. Trans. R. Soc. Lond. A 358 (1770), 1515–1532.
Poland, M.P., Sutton, A.J., Gerlach, T.M., 2009. Magma degassing triggered by static decompression at Kilauea Volcano, Hawai'i. Geophys. Res. Lett. 36, L16306. http://dx.doi.org/10.1029/2009GL039214.
Pompilio, M., Corsaro, R.A., Freda, C., Miraglia, L., Scarlato, P., Taddeucci, J., 2001. Petrological evidences of a complex plumbing system feeding the July–August 2001 eruption of Mt. Etna. Eos Trans. AGU 82 (47) (Fall Meet. Suppl., Abstract V52C-08).
Privitera, E., Bonanno, A., Gresta, S., Nunnari, G., Puglisi, G., 2012. Triggering mechanisms of static stress on Mount Etna volcano. An application of the boundary element method. J. Volcanol. Geotherm. Res. 245–246, 149–158.
Puglisi, G., Bonforte, A., Maugeri, S.R., 2001. Ground deformation patterns on Mount Etna, 1992 to 1994, inferred from GPS data. Bull. Volcanol. 62, 371–384. http://dx.doi.org/10.1007/s004450000112.
Puglisi, G., Bonforte, A., Ferretti, A., Guglielmino, F., Palano, M., Prati, C., 2008. Dynamics of Mount Etna before, during and after the July August 2001 eruption inferred from GPS and differential synthetic aperture radar interferometry data. J. Geophys. Res. 113, B06405. http://dx.doi.org/10.1029/2006JB004811.
Ratdomopurbo, A., Poupinet, G., 1995. Monitoring a temporal change of seismic velocity in a volcano: application to the 1992 eruption of Mt. Merapi (Indonesia). Geophys. Res. Lett. 22, 775–778.
Rymer, H., Murray, J.B., Brown, G.C., Ferrucci, F., McGuire, J., 1993. Mechanisms of magma eruption and emplacement at Mt. Etna between 1989 and 1992. Nature 361, 439–441.

Scandone, R., Cashman, K.V., Malone, S.D., 2007. Magma supply, magma ascent and the style of volcanic eruptions. Earth Planet. Sci. Lett. 253, 513–529.
Schiavone, D., Loddo, M., 2007. 3-D density model of Mt. Etna Volcano (Southern Italy). J. Volcanol. Geotherm. Res. 164, 161–175. http://dx.doi.org/10.1016/j.jvolgeores.2007.04.016.
Smith, W.H.F., Sandwell, D.T., 1997. Global seafloor topography from satellite altimetry and ship depth soundings. Science 277, 1957–1962.
Solaro, G., Acocella, V., Pepe, S., Ruch, J., Neri, M., Sansosti, E., 2010. Anatomy of an unstable volcano from InSAR: Multiple processes affecting flank instability at Mt. Etna, 1994–2008. J. Geophys. Res. 115, B10405. http://dx.doi.org/10.1029/2009JB000820.
Tait, S., Jaupart, C., Vergniolle, S., 1989. Pressure, gas content and eruption periodicity of a shallow crystallizing magma chamber. Earth Planet. Sci. Lett. 92, 107–123. http://dx.doi.org/10.1016/0012-821X(89)90025-3.
Tanguy, J.-C., Condomines, M., Kieffer, G., 1997. Evolution of Mount Etna magma: constraints on the present feeding system and eruptive mechanism. J. Volcanol. Geotherm. Res. 75, 221–250.
Tibaldi, A., Groppelli, G., 2002. Volcano-tectonic activity along structures of the unstable NE flank of Mt. Etna (Italy) and their possible origin. J. Volcanol. Geotherm. Res. 115, 277–302.
Trasatti, E., Giunchi, C., Piana Agostinetti, N., 2008. Numerical inversion of deformation caused by pressure sources: application to Mount Etna (Italy). Geophys. J. Int. 172, 873–884. http://dx.doi.org/10.1111/j.1365-246X.2007.03677.x.
Vinciguerra, S., Trovato, C., Meredith, P., Benson, P., 2005. Relating seismic velocities, thermal cracking and permeability in Mt. Etna and Iceland basalts. Int. J. Rock Mech. Min. Sci. 42, 900–910. http://dx.doi.org/10.1016/j.ijrmms.2005.05.022.
Walter, T.R., Acocella, V., Neri, M., Amelung, F., 2005. Feedback processes between magmatic events and flank movement at Mount Etna (Italy) during the 2002–2003 eruption. J. Geophys. Res. 110, B10205. http://dx.doi.org/10.1029/2005JB003688.
Yellin-Dror, A., Grassob, M., Ben-Avrahama, Z., Tiborc, G., 1997. The subsidence history of the northern Hyblean plateau margin, southeastern Sicily. Tectonophysics 282 (1–4), 277–289.